JACS
JOURNAL OF THE AMERICAN CHEMICAL SOCIETY

Article

pubs.acs.org/JACS

[FeFe]-Hydrogenase Oxygen Inactivation Is Initiated at the H Cluster 2Fe Subcluster

Kevin D. Swanson,[†,§] Michael W. Ratzloff,[‡,§] David W. Mulder,[‡] Jacob H. Artz,[†] Shourjo Ghose,[†] Andrew Hoffman,[†] Spencer White,[†] Oleg A. Zadvornyy,[†] Joan B. Broderick,[†] Brian Bothner,[†] Paul W. King,*[,‡] and John W. Peters*[,†]

[†]Department of Chemistry and Biochemistry, Montana State University, Bozeman, Montana 59717, United States

[‡]Biosciences Center, National Renewable Energy Laboratory, Golden, Colorado 80401, United States

Supporting Information

ABSTRACT: The [FeFe]-hydrogenase catalytic site H cluster is a complex iron sulfur cofactor that is sensitive to oxygen (O_2). The O_2 sensitivity is a significant barrier for production of hydrogen as an energy source in water-splitting, oxygenic systems. Oxygen reacts directly with the H cluster, which results in rapid enzyme inactivation and eventual degradation. To investigate the progression of O_2-dependent [FeFe]-hydrogenase inactivation and the process of H cluster degradation, the highly O_2-sensitive [FeFe]-hydrogenase HydA1 from the green algae *Chlamydomonas reinhardtii* was exposed to defined concentrations of O_2 while monitoring the loss of activity and accompanying changes in H cluster spectroscopic properties. The results indicate that H cluster degradation proceeds through a series of reactions, the extent of which depend on the initial enzyme reduction/oxidation state. The degradation process begins with O_2 interacting and reacting with the 2Fe subcluster, leading to degradation of the 2Fe subcluster and leaving an inactive [4Fe-4S] subcluster state. This final inactive degradation product could be reactivated *in vitro* by incubation with 2Fe subcluster maturation machinery, specifically $HydF^{EG}$, which was observed by recovery of enzyme activity.

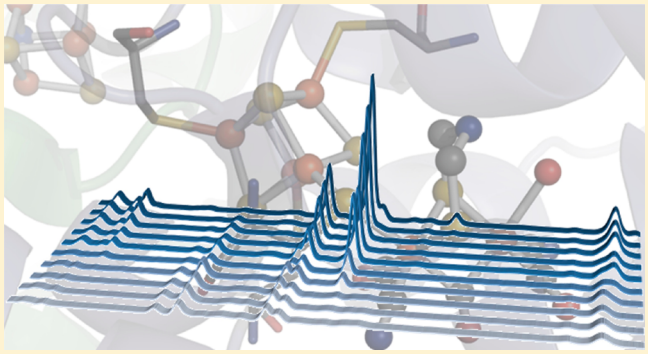

INTRODUCTION

[FeFe]-hydrogenases are found in bacteria and lower eukaryotes and are commonly involved in the recycling of reduced electron carriers that accumulate during anaerobic metabolism.[1] [FeFe]-hydrogenases catalyze reversible H_2 activation at very high rates and thus are attractive targets for bioengineering efforts aimed at coupling microbial H_2 production to oxygenic photosynthesis.[2,3] The proton reduction reaction in [FeFe]-hydrogenases occurs at a complex bridged FeS cluster termed the H cluster.[4,5] The H cluster exists as a regular [4Fe-4S] subcluster bridged to an organometallic, 2Fe subcluster through a protein cysteine thiolate. The 2Fe subcluster is coordinated by unique nonprotein ligands including CO, CN, and dithiomethylamine (Figure 1).[4−8]

A major barrier to utilization of [FeFe]-hydrogenases for photosynthetic H_2 production is they are rapidly inactivated upon exposure to O_2, the byproduct of water oxidation.[9−11] However, [FeFe]-hydrogenases from different sources vary significantly in the level of sensitivity,[12−16] and understanding the basis for this variation may provide insight into addressing this limitation. One hypothesis to account for the variation is from structural differences controlling the initial access or

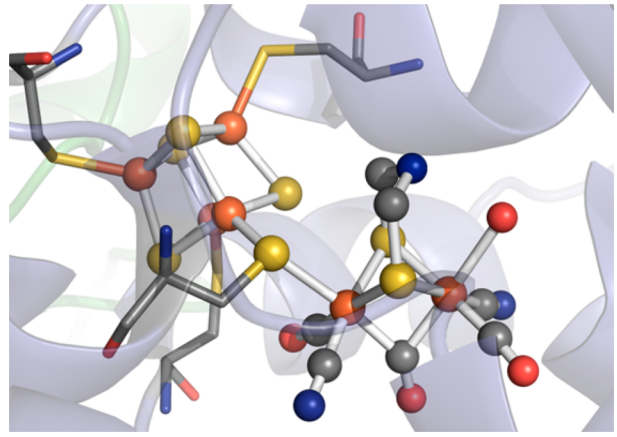

Figure 1. H cluster ball-and-stick representation with carbon, nitrogen, oxygen, sulfur, and iron atoms colored gray, blue, red, yellow, and orange, respectively (PDB 3C8Y).

Received: October 9, 2014
Published: January 12, 2015

DOI: 10.1021/ja510169s
J. Am. Chem. Soc. 2015, 137, 1809−1816

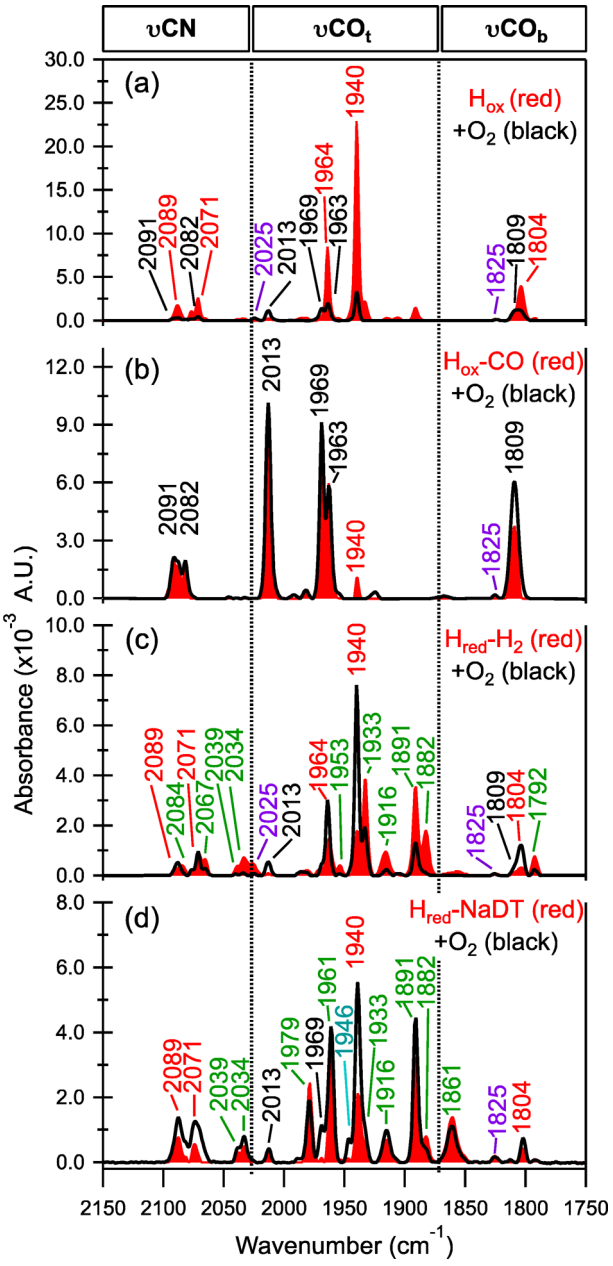

Figure 2. FTIR spectra of CrHydA1 samples exposed to O_2. The solid red spectra are prior to O_2 injection, and black traces after 2 h exposure to O_2 at pH 8, 277 K. (a) H_{ox}, ~0.01% O_2; (b) H_{ox}-CO, ~2.4% O_2; (c) H_{red}-H_2, ~0.01% O_2; (d) H_{red}-NaDT, ~0.05% O_2. Wavenumbers assignments: H_{ox}, red; H_{ox}-CO, black; H_{red}-NaDT and H_{red}-H_2, green; O_2 damaged, purple; and unassigned, cyan. Additional experimental conditions are described in the Experimental Section.

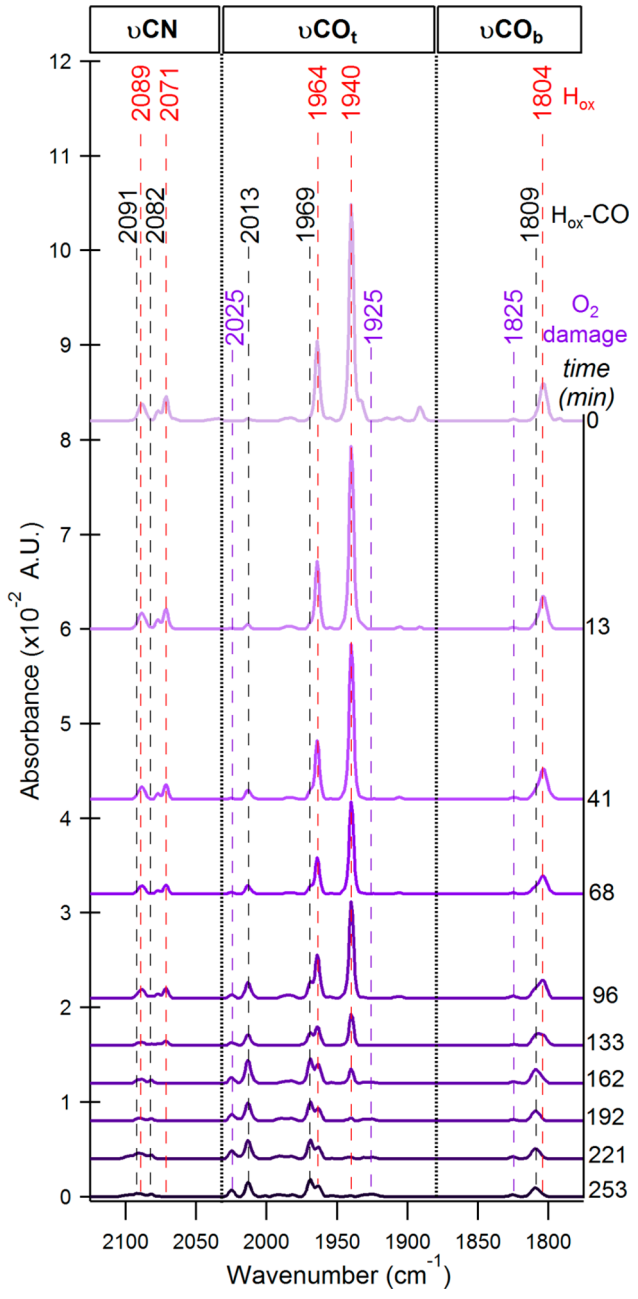

Figure 3. Time course of the FTIR spectra of H_{ox} CrHydA1 exposed to ~0.01% O_2 at pH 8, 277 K. The initial H_{ox} signal (1804, 1940, 1964, 2071, and 2089 cm^{-1}) gradually decays, and the spectrum transitions to a characteristic H_{ox}-CO signal with νCO peaks at 1809, 1963, 1969, and 2013 cm^{-1}. Signals assigned to O_2 damaged clusters are shown in purple. Additional experimental conditions are described in the Experimental Section.

transport of O_2 to the H cluster.[15,17,18] Support for this comes from computational studies that have revealed putative hydrophobic channels proposed to function in the diffusion of gases, including O_2, to and from the active site.[17,19] In addition to O_2 access, density functional theory (DFT) has been employed as a means to probe the binding and reaction steps that subsequently result in O_2-dependent enzyme degradation. Binding models suggest that initiation of O_2 interaction with the H cluster differs between enzymes and is dependent on H cluster oxidation state.[20−22] The O_2 binds at the H cluster distal Fe (Fe_d) to result in formation of "transient" -OOH or -O_2^- terminal species. Further reaction cycles of the terminal "O" species with H^+ generate H_2O_2 or Fe-peroxide.[21,23]

The computational models of the O_2 inactivation process require further validation but suggest reactions with O_2 are dependent on availability of both protons and electrons.[23,24] Hints at the chemical nature of the O-species produced from O_2 reactions at the H cluster have come from electrochemical studies of O_2 reduction by a 2Fe subcluster model complex. The subcluster was found to reduce O_2 to ROS (i.e., H_2O_2) and catalyzed the complete 4e$^-$ reduction to H_2O, the extent of which was dependent on pH, potential, and scan rate. The 2Fe

DOI: 10.1021/ja510169s
J. Am. Chem. Soc. 2015, 137, 1809−1816

subcluster degradation pathways also included FeS oxidation (e.g., Fe-oxidation and S-oxygenation).[25] These results together with DFT calculations on O_2 products imply that the [FeFe]-hydrogenases might also catalyze the reduction of O_2 as a substrate where differences in proton/electron availability may account for the differences in sensitivity among enzymes.[23,25]

Inactivation of the [FeFe]-hydrogenases has also been studied by electrochemical methods.[13−16,26,27] Aerobic, O_2 inactivation was shown to be a potential-dependent process and that the presence of CO or H_2 affords a protective effect via competitive binding to Fe_d of the 2Fe subcluster. Anaerobic, oxidative inactivation of [FeFe]-hydrogenases has been observed at potentials >65 mV (vs SHE) in the presence of H_2 and was modeled by DFT to involve reversible and irreversible structural rearrangements of the H_{ox} state.[26] Irreversible inactivation occurred at more positive potentials and was modeled as a slow oxidation of H_{ox} followed by nucleophilic attack and degradation.[26] Whether aerobic inactivation involves similar redox-induced rearrangements remains to be determined. Structural and biophysical studies on O_2 reactions with the H cluster are challenging, and reports are limited.[13,14] A mechanistic model from X-ray absorption spectroscopy (XAS) studies on CrHydA1 proposes that O_2 reactions with the H cluster produce ROS that results in the initial destruction of the [4Fe-4S] subcluster.[27,28] This model accounts for the protective effect of CO (which prevents O_2 binding at the 2Fe subcluster) but conflicts with conclusions from DFT whereby O_2 reacts with 2Fe subcluster to form ROS or other oxidation products that initially degrade the 2Fe sub cluster, not the [4Fe-4S] subcluster.[21,23]

The models that have emerged from computational and experimental studies have led to some controversy as to the nature of O_2-dependent inactivation of [FeFe]-hydrogenases and mechanism of H cluster degradation.[29] In order to resolve uncertainties on the mechanism of O_2 inactivation of [FeFe]-hydrogenases, we have exposed the [FeFe]-hydrogenase from *Chlamydomonas reinhardtii* (CrHydA1) to different titers of O_2 while monitoring changes in the biochemical activities and Fourier transform infrared (FTIR) and UV−vis spectroscopic properties. The FTIR results indicate that H cluster reacts with O_2 and undergoes a series of reactions to produce a mixture of inactivation intermediates, the populations of which depend on the initial reduction/oxidation state of the H cluster. Ultimately, oxidative destruction results in the loss of the 2Fe subcluster and formation of a [4Fe-4S] subcluster intermediate state. This inactivation/degradation intermediate could be reactivated *in vitro* by incubation with the 2Fe subcluster-specific maturation machinery.

EXPERIMENTAL SECTION

Protein Preparation. Heterologous expression and purification of CrHydA1 in *Escherichia coli* was performed as previously described.[30,31] The protein was purified under anaerobic conditions in an MBraun anaerobic chamber (MBraun USA). All buffers were gas exchanged under repeated cycles of vacuum and O_2-free gas prior to purification. CrHydA1 isolation from cell extracts was performed using a two-step chromatography process of ion-exchange over diethylaminoethanol (DEAE, GE Lifesciences) Sepharose followed by affinity capture on Strep-Tactin (IBA) resin.[31] Strep-Tactin bound enzyme was eluted in 50 mM Tris buffer (pH 8.0) containing 300 mM NaCl, 5% glycerol, 5 mM sodium dithionite (NaDT), and 2 mM desthiobiotin. Purity was verified by sodium dodecyl sulfate polyacrylamide gel electrophoresis (SDS-PAGE), and the concentration determined by Bradford assay. CrHydA1 was prepared in the oxidized (H_{ox}) state by serial concentration and dilution in NaDT-free buffer until the FTIR spectra consisted primarily of H_{ox}.

HydF was obtained by expression of *hydF* in the background of HydE and HydG ($HydF^{EG}$) in *E. coli* strain BL21 (DE3). The *hydE*, *hydF*, and *hydG* from *Clostridium acetobutylicum* were individually cloned into pET-Duet, pRSF-Duet, and pCDF-Duet, respectively.[32] The cloned copy of *hydF* contained a N-terminal 6xHis tag.[32] Cells were grown in LB Miller growth medium supplemented with streptomycin (50 mg L^{-1}), kanamycin (30 mg L^{-1}), ampicillin (100 mg L^{-1}), 0.5% w/v glucose (~25 mM), 2 mM ferric ammonium citrate, and 50 mM phosphate buffer (final pH of medium was 7.4). All cultures were grown aerobically at 25 °C until an OD_{600} of 0.5. Cultures were sparged with 100% argon for 20 min and induced with 1.5 mM isopropyl β-D-1-thiogalactopyranoside (IPTG). Cysteine (2 mM) and sodium fumarate (25 mM) were added immediately after IPTG addition. For expression under anaerobic conditions, cultures were sparged with argon at 25 °C overnight.

$HydF^{EG}$ was purified in an anaerobic chamber (Coy Laboratories, Grass Lake, MI) as previously described.[32] Cells were harvested by centrifugation and cell pellets stored at −80 °C. Cells were lysed by resuspension in buffer composed of 10 mM HEPES, pH 7.4, 0.5 M KCl, 5% glycerol, 1 mM dithiothreitol, 20 mM imidazole, 20 mM $MgCl_2$, 1 mM PMSF, 1% Triton X-100, 140 μg mL^{-1} DNase and RNase, and 120 μg mL^{-1} lysozyme. The cell lysate was stirred for 1 h at room temperature and centrifuged in gastight bottles at 38,000 × *g* for 30 min. The His-$HydF^{EG}$ was purified from the supernatant by immobilized metal chromatography on a TALON cobalt column (GE Life Sciences). The column was loaded and washed with 15 column volumes of 20 mM HEPES pH 7.4, 0.5 M KCl, 5% glycerol, 1 mM dithiothreitol, and 20 mM imidazole. Purified $HydF^{EG}$ was eluted with 200 mM imidazole. $HydF^{EG}$ was collected and concentrated anaerobically with 30 kDa Amicon Ultra-15 centrifugal concentrators (Millipore). The $HydF^{EG}$ was loaded onto a G25 PD-10 desalting column (GE Life Sciences) to remove imidazole and eluted with 50 mM HEPES pH 7.4, 0.5 M KCl, 5% glycerol, and 1 mM dithiothreitol. Purified $HydF^{EG}$ was flash frozen in liquid N_2 and stored at −80 °C or in liquid N_2 until further use.

Preparation of Oxygen Treated CrHydA1. O_2 gas standards were prepared using septum-sealed 123 mL Wheaton vials. Dilutions were prepared using a gastight syringe (Hamilton) to remove gas from a 100% O_2 standard (equilibrated to atmospheric pressure) and injecting the O_2 into vials containing 100% N_2 at atmospheric pressure. Standards of 100%, 4%, 1%, and 0.1% O_2 were used for all of the O_2 additions. Samples used to measure the FTIR spectra of O_2 treated CrHydA1 were prepared as follows. H_{ox} (Figures 2 and 3): O_2 was injected by gastight syringe into the headspace above an 75 μL aliquot of oxidized CrHydA1 at 45 mg mL^{-1} in a septum-sealed 825 μL conical vial. CO-inhibited (H_{ox}-CO): a 15 μL aliquot of 70 mg mL^{-1} H_{ox} CrHydA1 was injected via gastight syringe into a septum-sealed 825 μL conical vial that had previously been flushed with 100% CO. O_2 was then injected by gastight syringe into the headspace of the conical vial (Figures 2 and S1). H_2 reduced (H_{red}-H_2) (Figure 2): 70 μL of 30 mg mL^{-1} H_{ox} CrHydA1 in a septum-sealed 825 μL conical vial, along with three similar empty conical vials, underwent 10 vacuum/100% H_2 exchanges on a Schlenk line and was incubated for 1 h at 4 °C in the Mbraun. A 10 μL aliquot of this enzyme sample was transferred to each one of the empty, H_2-treated vials via gastight syringe. O_2 was then injected by gastight syringe into the headspace of each vial. NaDT-reduced (H_{red}-DT) (Figures 2 and S2): in the MBraun glovebox, NaDT (20 mM final) was added to 50 μL of 50 mg mL^{-1} H_{ox} CrHydA1 (45 mg mL^{-1} final) and mixed via pipetting for 30 s. A 15 μL aliquot was transferred to a 825 μL conical vial and then sealed with a septum. O_2 was injected by gastight syringe into the headspace of the conical vials.

In all cases, the conical vials contained a microstir bar and were stirred while on an ice bath. Final O_2 concentrations ranged from 0.01 to 24.7% (v/v). In order to minimize pressure increases due to gas injection, the appropriate standard was used to keep the injection volume <5% of the vial volume (with the exception of the 24.7% CO sample shown in Figure S1). An aliquot of CrHydA1 was removed

DOI: 10.1021/ja510169s
J. Am. Chem. Soc. 2015, 137, 1809−1816

from the septum-sealed vial using gastight syringe and loaded in a custom gastight FTIR sample cell.[33] A summary of the O_2 concentration and molar ratios is given in Table S1. Control experiments were performed to estimate the repeatability of O_2 injections, with O_2 concentrations determined by GC (Agilent Technologies). The standard deviation for O_2 injections is estimated to be SD = ±(% O_2 × 0.15) or ±15% of each individual injection (Table S2).

FTIR Spectroscopy. Spectra were collected as described previously with a Nicolet 6700 FTIR spectrometer (Thermo Fisher Scientific) equipped with a Globar IR source, a CaF_2 beam splitter, and a liquid-nitrogen-cooled mercury cadmium telluride (MCT) detector.[33] All of the spectra were collected at room temperature (21 °C). The custom-built sample chamber consists of a covered aluminum box designed to minimize external light interference with the sample. The OMNIC software was configured to report absorbance spectra, and absorbance baselines were fit to these data using a manually adjusted spline.

UV−vis Spectroscopy. A 100 μL aliquot of 3 mg mL^{-1} H_{ox} CrHydA1 was prepared in the glovebox under 100% N_2, transferred into low volume 1 cm path-length quartz cuvette, and septum sealed. The O_2 reaction was initiated by injecting O_2 (at 0.001%, 17%, or 300%) with a gastight syringe into the headspace of cuvette with the enzyme solution at 4 °C, cooled with a Peltier cooler. A microstir bar provided agitation of the solution in the cuvette. The reaction of CrHydA1 with O_2 was monitored by UV−vis every min for 200−300 min, by scanning over a 250−750 nm range at 1 nm intervals. UV−vis spectra were recorded on a Cary 4000 UV−vis spectrophotometer.

Activity Assays. Activities of CrHydA1 were assayed by H_2 evolution from reduced methyl viologen. Reaction volumes of 0.6 or 2 mL were placed in 3 or 10 mL Wheaton vials containing 5 mM methyl viologen (MV), 10 mM NaDT, 50 mM Tris, 300 mM NaCl, 5% glycerol, and between 25 ng and 4 μg of enzyme per assay. Hydrogen production was detected by gas chromatography (Agilent Technologies).

Mass Spectrometry. Protein digests were performed with 1.5 mg mL^{-1} CrHydA1, 12.5 ug mL^{-1} Trypsin Gold (Promega), 50 mM Tris-HCl pH 8, 300 mM NaCl, and 5% glycerol. Reactions were incubated overnight in a 37 °C heat block, and complete digestion was verified by SDS-PAGE. The digestion product was diluted up to a 1000-fold in 50/50 water/acetonitrile and transferred to screw capped auto sampler vials for LCMS.

An Agilent 1100 series HPLC system coupled to an Agilent Chip Cube integrated microfluidics reverse-phase nano-HPLC system was used. Trapping and analytical separations were performed with an Agilent C18 HPLC-Chip (G4240-62001, 40 nl trap column and 75 μm × 43 mm analytical). Chromatography solvents were H_2O with 0.1% (v/v) formic acid for channel "A" and acetonitrile for channel "B". The HPLC program was held at 7% B from 0.0 to 2.0 min, then ramped from 7 to 35% B from 2.0 to 20.0 min. The gradient was then ramped from 35 to 95% B from 22 to 27 min. The mass spectrometer was an Agilent 6520 Q-TOF with a dual-ESI source: resolution approximately 20,000 and accuracy 3 ppm. Spectra were collected in positive mode from 50 to 1700 m/z at 2 Hz for both MS and MS/MS, with adaptive acquisition time for highly abundant ions.

The resulting MS/MS data were analyzed using the PEAKS 6.0 software package and searching the CrHydA1 protein sequence. Peptide mass tolerance was 10 ppm and fragment mass tolerance 0.5 Da. Variable modifications were set to sulfonic acid 47.97, sulfinic acid 31.98, and oxidation or hydroxylation of cysteine 15.99.

Crystallization and Structure Determination. CrHydA1 (1 mL at 10 mg mL^{-1}) in NaDT free buffer was exposed to 0.01% O_2 for 2 h in a 4.5 mL Wheaton vial. Enzyme activity was measured at the end of the 2 h period (50 μmol min^{-1} mg^{-1}). An aliquot of the sample was set aside for trypsin digest and MS analysis, and the rest of the sample was concentrated to 30 mg mL^{-1} for crystallization. CrHydA1 was crystallized anaerobically in a MBraun glovebox at room temperature using microcapillary batch diffusion with a precipitation solution of 25.5% polyethylene glycol 8000 as precipitate and 0.085 M sodium cacodylate (pH 6.5), 0.17 M sodium acetate trihydrate, and 1 mM dithionite. After allowing the crystals to form for 2−3 weeks, they were mounted on cryo-loops and flash frozen in liquid nitrogen. Data were collected at the Stanford Synchrotron Radiation Lightsource (SSRL) on beamline BL12-1 at 1.75 Å wavelength. The data was processed using XDS[34] and scaled with Pointless and Aimless.[35] The structure was solved using molecular replacement using AutoMR (CCP4 suite of programs) with CrHydA1 (PDB ID, 3LX4).[36] The structure was built using COOT with further refinement using REFMAC5 using NCS and B factor restraints. The final model was solved to 2.23 Å with an R factor of 24.1% and an R free of 27.7% (Table S5). Atomic coordinates were deposited in the PDB (code 4ROV).

***In vitro* Reactivation of O_2 Inactivated CrHydA1.** Reactivation of the O_2 inactivated CrHydA1 was performed with the addition of N-terminal His tagged-$HydF^{EG}$ at different molar ratios to obtain a 300 μL total volume in 3 mL crimp sealed anaerobic Wheaton vials. CrHydA1 was allowed to reactivate at 37 °C in a water bath for 1 h, and reactivation was followed by measuring the H_2 production activity as described above.

RESULTS

FTIR Analysis and Comparison of Oxidized, Reduced, and CO-Inhibited CrHydA1. The H cluster oxidation state and 2Fe subcluster site occupancy are known to affect the process of O_2 damage. To test whether FTIR can also detect changes in O_2 damage of the 2Fe subcluster, the reducing agents sodium dithionite (NaDT) and H_2 and the competitive inhibitor CO were each added to oxidized (H_{ox}) CrHydA1, and the samples exposed to O_2 and monitored by FTIR. CrHydA1 prepared in the H_{ox} state has major peaks at 1804, 1940, 1964, 2071, and 2089 cm^{-1} (Figure 2a, red spectrum). Exposure of the H_{ox} CrHydA1 to ∼0.01% O_2 (Figure 2a, black spectrum) for 2 h resulted in the loss of H_{ox} features and an increase in features assigned to CO-inhibited (H_{ox}-CO) and O_2-damaged H cluster. By comparison, a control time-course experiment (Figure S3) on a duplicate CrHydA1 sample in the absence of O_2 showed only slight changes in the intensity of the H_{ox} signal, which increased presumably due to auto-oxidation of H_{red}.

When H_{ox} CrHydA1 was exposed to CO to make H_{ox}-CO (Figure 2b, red spectrum), the νCO and νCN peaks shifted to higher wavenumbers (νCO at 1809, 1963, 1969, 2013, and νCN at 2082 and 2091 cm^{-1}) as was previously reported for CO-inhibited [FeFe]-hydrogenases.[33,37−39] The enzyme was then exposed to ∼2.4% O_2. H_{ox}-CO was exposed to larger percentages of O_2 in order to determine whether attenuation of FTIR signal could be observed. After approximately 2 h of O_2 exposure, the FTIR spectrum indicated the peaks assigned to H_{ox}-CO remained relatively unchanged (Figure 2b, red vs black spectrum). Small peaks appeared, which are attributed to degradation of some residual H_{ox} species. Enzyme in the H_{ox}-CO state was also treated with higher amounts of O_2 (up to ∼24.7%, Figure S1), and the resulting FTIR spectrum again showed significantly less degradation compared to H_{ox} and H_{red} preparations, consistent with previous observations that H_{ox}-CO is more resistant to oxidative reactions with O_2.[14,15,27,40]

Equilibration of H_{ox} CrHydA1 under 100% H_2 led to a collective shift in the νCO peaks, consistent with ligand exchange and electronic transitions at the H cluster associated with H_2 activation as previously described.[33,41] Figure 2c shows the spectrum of H_2-reduced CrHydA1 with principle νCO peaks, assigned to a mixed population of reduced intermediates, observed at 1792, 1882, 1891, 1916, 1933, 1953, and 1963 cm^{-1} (Figure 2c, red spectrum).[33,41,42] Additional low intensity H_{ox}-CO peaks were seen in this sample, possibly arising from a slight amount of O_2 exposure during H_2 treatment. Exposure of H_{red}-H_2 CrHydA1 to ∼0.01% O_2 for 2 h, in the presence of

DOI: 10.1021/ja510169s
J. Am. Chem. Soc. 2015, 137, 1809−1816

100% H_2 atmosphere, led to attenuation of the 1792, 1882, 1891, 1916, and 1933 cm^{-1} peaks (Figure 2c, red vs black spectrum) accompanied by an increase in peak intensities assigned to H_{ox} at 1804, 1940, and 1964 cm^{-1} together with a small increase in peak intensities assigned to H_{ox}-CO at 1969 and 2013 cm^{-1}.

When H_{ox} CrHydA1 was treated with NaDT (20 mM final concentration), the initial spectrum (Figure 2d, red spectrum) showed νCO peaks at 1861, 1882, 1891, 1916, 1961, and 1979 cm^{-1} previously assigned to reduced intermediates.[33,41,42] Compared to H_{ox} (Figure 2a), the NaDT-treated CrHydA1 showed less signal attenuation after exposure to O_2 (Figure 2d, red vs black spectra), with only a small loss of 2Fe subcluster signal after 2 h of exposure to ~0.05% O_2. Regarding νCO peak intensities, the O_2 treatment produced new peaks at 1946 and 1969 cm^{-1}, a slight increase in peak intensities at 1916 and 2013 cm^{-1}, and larger increases in peak intensities at 1804 and 1940 cm^{-1}. The increases at 1804 and 1940 cm^{-1} are assigned to an increase in the population of H_{ox}, and the changes at 1969 and 2013 cm^{-1} are assigned to an increase in the population of H_{ox}-CO. The appearance of H_{ox} is similar to the sequence observed for O_2 exposure of H_2-reduced CrHydA1 (see Figure S2).

FTIR Time Series of O_2 Exposed H_{ox} CrHydA1. In order to observe O_2-induced transitions in the 2Fe subcluster by FTIR on the time scales of full spectral collection (512 scans, ~8 min), CrHydA1 prepared in the H_{ox} state (with νCO modes at 1804, 1940, 1964 cm^{-1}) was incubated under a low (~0.01%) O_2 partial pressure at 4 °C, and FTIR spectra were collected at approximately 25 min intervals (Figure 3). Based on an O_2 titration series (Figure S4) we selected 0.01% O_2 for the time-course experiment in order to allow the time scales of oxidative transitions to match the time frame of IR sampling and data collection. Under 0.01% O_2, the H_{ox} signal gradually attenuated, which coincided with the appearance of H_{ox}-CO with νCO peaks at 1809, 1963, and 2013 cm^{-1}. A near complete loss of H_{ox} was observed after ~200 min of O_2 exposure. The calculated decay rates of H_{ox} specific νCO signal at 1940 cm^{-1} directly correlated with inactivation rates (values are shown in Tables S3 and S4).

We also measured the change in the FTIR spectra of *Clostridium acetobutylicum* HydA (CaI) prepared in H_{ox} and exposed to a ~30-fold higher concentration (~0.28%) of O_2. This enzyme is ~100-fold less sensitive to O_2 inactivation than CrHydA1,[15] thus was expected to have slower kinetics of O_2-induced changes in FTIR spectral features. A time-course spectrum series (Figure S5) of CaI exposed to ~0.28% O_2 shows a slower decay of H_{ox} peak intensities (Tables S3 and S4) and slower appearance of H_{ox}-CO signals, than for CrHydA1.

The amount of O_2-treated H_{ox} CrHydA1 that converted to H_{ox}-CO was determined based on normalizing the νCO peak intensities in the O_2-treated sample to the H_{ox}-CO standard (Figure 2b, red spectrum). The amount of H_{ox}-CO was estimated at ~20% after 133 min (Figure 4a) of ~0.01% O_2 exposure, where the rest of the signal loss is likely due to complete degradation of the 2Fe subcluster, which is observed at 253 min (Figure 4b). The O_2-induced H_{ox}-CO signal appeared simultaneously with the loss of H_{ox} and slowly decreased in intensity after 133 min (Figure 3). After a longer period of exposure, the loss of H_{ox}-CO was accompanied by the appearance of new νCO peaks at 1825, 1925, and 2025 cm^{-1} (Figure 4b).

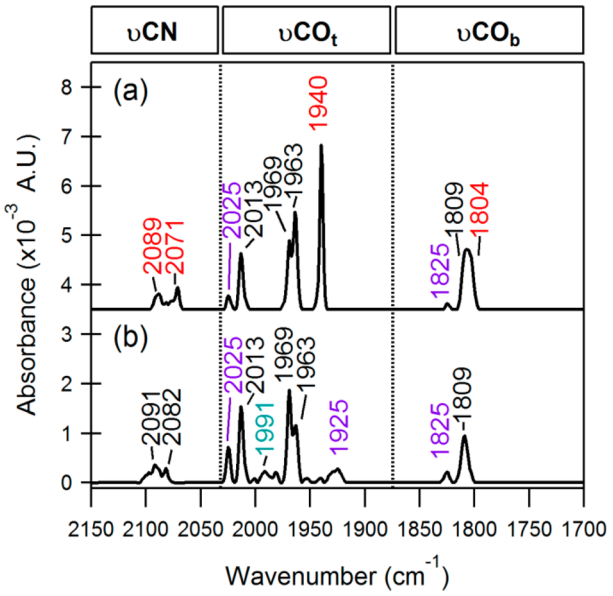

Figure 4. FTIR spectra of H_{ox} CrHydA1 after long-term exposure to 0.01% O_2, pH 8, 277 K. Scans taken at (a) 133 and (b) 253 min, after exposure to O_2. Wavenumber coloring is as described in Figure 2.

The putative νCO bands at 1825, 1925, and 2025 cm^{-1} might arise from oxygenation of a bridging thiolate, which was observed to induce a 6–19 cm^{-1} upshift of the νCO IR bands.[43] It is possible that O_2 or a byproduct of O_2 led to a similar effect on CrHydA1 νCO bands (see Figure 4a,b).[43] In depth DFT calculations on O_2 binding to the H cluster propose reaction pathways that include both oxygenation of Fe_d and oxidation of 2Fe.[20,21,23,44,45] In this case, the resulting oxidation of the 2Fe subcluster would be expected to cause an upshift in the νCO bands, again consistent with the observed upshifts in CrHydA1 H_{ox} spectrum after O_2 exposure.

UV–vis of O_2 Exposed CrHydA1. UV–vis spectroscopy was employed to monitor the [4Fe-4S] cluster during O_2 exposure. The absorption spectra of holo-CrHydA1, CrHydA1 expressed in the absence of HydE, HydF, and HydG and lacking the 2Fe subcluster (CrHydA1$^{\Delta EFG}$), and the O_2 inactivated CrHydA1 all showed a broad 415–420 nm absorbance feature associated with S → Fe charge-transfer bands of FeS clusters. CrHydA1$^{\Delta EFG}$ contains only a [4Fe-4S] subcluster inserted by *E. coli's* FeS cluster assembly machinery.[46,47]

Inactivation of CrHydA1 by exposure to ~0.001% and 17% O_2 for 2 h was monitored by H_2 evolution activity and UV–vis spectroscopy. The initial activity was 500 μmol $min^{-1}mg^{-1}$, which declined after the 2 h 0.001% O_2 treatment to 12 μmol min^{-1} mg^{-1}. CrHydA1 that was not exposed to O_2 did not show a decrease in specific activity nor any change in the UV–vis spectra. The blue trace in Figure 5b,c is the starting spectrum of holo-CrHydA1, and the black trace is after 2 h incubation with 0.001% O_2, the brown trace is after 2 h incubation with 17% O_2. The difference spectra between holo-CrHydA1 (Figure 5b,c, blue trace) and O_2 inactivated CrHydA1 (Figure 5b,c, black and orange traces) did not reveal significant differences (data not shown), suggesting that most of the S → Fe charge-transfer absorption is maintained after O_2 inactivation. This result is consistent with stability of the [4Fe-4S] cluster against O_2 damage. CrHydA1 that was exposed to large amounts of O_2 (3 atm of 100% O_2 for 3 h) exhibited

DOI: 10.1021/ja510169s
J. Am. Chem. Soc. 2015, 137, 1809–1816

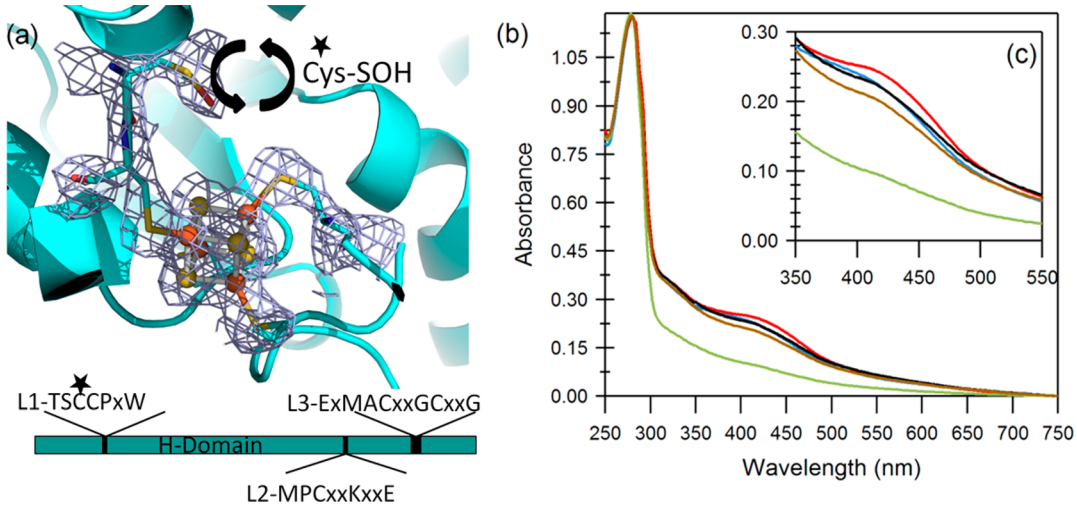

Figure 5. Crystal structure and UV−vis of O_2 inactivated CrHydA1. (a) Electron density map contoured at 2σ showing extra electron density in the H cluster environment including oxidized Cys 169. The conserved [FeFe]-hydrogenase motifs are depicted below the ribbon diagram with Cys 169 (starred). Reactions with O_2 were conducted at pH 8, 298 K. (b) The full spectrum of reduced immature CrHydA1$^{\Delta EFG}$ (red line), and of holo-CrHydA1 (blue line) after inactivation with 0.001% O_2 2 h (black line), after inactivation with 17% O_2 2 h (dark-red line), or with 3 atm of 100% O_2 for 3 h (green line). (c) A close-up view of the 350−550 nm region. Reactions with O_2 were conducted at pH 8, 277 K.

significant decay in the peak at 420 nm (Figure 5b,c, green trace) consistent with the loss of S → Fe charge-transfer bands of FeS clusters.

***In-vitro* Activation of O_2 Inactivated CrHydA1.** CrHydA1 that had been O_2 inactivated could be *in vitro* reactivated with HydF^{EG} (Figure S7) to ∼80% of the as-purified activity level. The remaining population of enzyme that could not be re-activated was likely degradation products that do not have an intact [4Fe-4S] cluster.[48] This data suggests there is a significant population of enzyme (∼80%) containing intact [4Fe-4S] after O_2 exposure. It had been previously shown that HydF^{EG} is sufficient for activating CrHydA1$^{\Delta EFG32}$ and that activation of CrHydA1$^{\Delta EFG}$ requires the assembly of a preformed [4Fe-4S] cluster.[46]

Structural Characterization of O_2 Inactivated CrHydA1. CrHydA1 inactivated by O_2 readily crystallized, and the structure was determined to ∼2.3 Å resolution. The resulting structure was very similar to the previously characterized structure of purified CrHydA1 expressed in the absence of [FeFe]-hydrogenase maturases HydE, HydF, and HydG with an overall root-mean-squared deviation between the two structures of 0.29 Å.[46] The structure revealed a vacant 2Fe subcluster site and an intact [4Fe-4S] subcluster (Figure 5a) and an open channel leading from the surface to the site left vacant in absence of the 2Fe subcluster. This suggests that the O_2 inactivated CrHydA1 is the appropriate conformation and is consistent with the observation that O_2 inactivated CrHydA1 can be reactivated by the H cluster maturation machinery. In addition, the structure revealed three Cys residues (amino acids 88, 169, and 238) to have additional electron density around the sulfur atoms, which can be modeled and refined suggesting sulfenic acid at position Cys 169 (which functions in proton-transfer to the H-cluster).[49,50] Sulfenic acid was modeled at position 169 in two conformations at 0.7 and 0.3 relative occupancies. The relative *B* factors of oxygen were in line with those of the adjacent sulfur in both conformations indicating complete oxidation of Cys 169. Similar electron density was observed for surface localized Cys 238 and Cys 88 also presumed to be oxidized. No modifications of the four Cys residues that function to coordinate the H cluster (Cys 170, 225, 417, and 421) were detected. Due to the functional importance of Cys 169,[49,50] mass spectometry (MS) analysis was used to confirm the presence of sulfenic acid at the Cys 169 position (Figure S6).

■ DISCUSSION

FTIR analysis of CrHydA1 incubated in the presence of ∼0.01% O_2 and in the absence of exogenously added reducing agents exhibited attenuation of the H_{ox} state. The attenuation of the H_{ox} signal tracked closely with the loss of enzyme activity. A detectable level of H_{ox}-CO signal appeared with the loss of the Hox signal, suggesting degradation of the 2Fe subcluster liberates CO that in turn binds to the remaining intact H clusters, generating H_{ox}-CO.

The changes that occur when CrHydA1 was exposed to O_2 appear to occur to a greater extent and at a higher rate when poised in the H_{ox} state. Enzymes poised in H_{ox}-CO, H_{red}-H_2, and H_{red}-NaDT were less prone to O_2-dependent decay. The data show that an H cluster that is presumably coordinately saturated with an occupied Fe_d ligand exchangeable site is more resistant to O_2 damage consistent with this site as the initial site of O_2 binding and attack along the pathway of H cluster degradation.[13−15,21,22,26,27] The addition of CO had the greatest protective effect with no observable decay of H_{ox}-CO up to 24.7% O_2 (Figure S1) over 2 h of exposure, consistent with previous electrochemical observations.[14,15,27] The reduced samples showed a clear transition to H_{ox} (1940 cm^{-1} νCO) prior to signal decay and H cluster degradation. Subsequently, similar degradation products are observed in the NaDT- and H_2-treated CrHydA1 samples as were observed with H_{ox} samples, with the transient appearance of H_{ox}-CO-specific FTIR features.

The O_2 inactivated CrHydA1 was capable of being reactivated by the addition of HydF^{EG} suggesting that the inactivated enzyme has a damaged or absent 2Fe subcluster. Further, as described above, both UV−vis spectroscopy and structural characterization indicated the presence of an intact [4Fe-4S] subcluster that was stable long after activity

DOI: 10.1021/ja510169s
J. Am. Chem. Soc. 2015, 137, 1809−1816

attenuated. Interestingly, the X-ray crystal structure and UV−vis of O_2 inactivated CrHydA1 strongly resembled CrHydA1 expressed in the absence of maturases ($CrHydA1^{\Delta EFG}$). Previous studies probing H cluster degradation using comparatively higher concentrations of O_2 either with[28] or without[27] NaDT proposed that the degradation of the [4Fe-4S] subcluster preceded 2Fe subcluster degradation, whereby ROS was generated by O_2 binding and reaction at the 2Fe subcluster. Under the conditions of our study in which CrHydA1 was exposed to O_2 in the absence of NaDT, the [4Fe-4S] subcluster seems fairly resistant to degradation (see Figure 5). We do however observe evidence for the oxidation of the non-coordinating active site Cys (Cys 169) perhaps through the formation of ROS. These results further support the formation of ROS species in the pathway of O_2 inactivation and highlight the apparent resilience of the [4Fe-4S] subcluster to O_2 initiated degradation relative to the 2Fe subcluster. Exposure of either the O_2 degradation intermediate observed here or $CrHydA1^{\Delta EFG}$ to high concentrations of O_2 resulted in the eventual destruction of the [4Fe-4S] subcluster, as evidenced by reduction and eventual loss of the S → Fe charge-transfer bands at ∼420 nm.

Thus, based on the experimental evidence presented here, we propose that the mechanism of O_2 attack on CrHydA1 first involves degradation of the more labile 2Fe subcluster, followed by attack on the more robust [4Fe-4S] subcluster.

CONCLUSION

The inactivation of [FeFe]-hydrogenase by O_2 is defined by steps that involve the diffusion of gases into close proximity of the catalytic site, followed by redox and chemical reactions of O_2 with the H cluster. Our results are consistent with theoretical models[21] that the latter process leads to oxidative breakdown of the 2Fe subcluster and eventual formation of a stable [4Fe-4S] subcluster product with a vacant 2Fe subcluster site. This product was capable of being reactivated by 2Fe subcluster-specific maturation machinery. Long-term and/or high-concentration O_2 exposure is required for oxidative damage of the [4Fe-4S] subcluster and complete H cluster degradation.

ASSOCIATED CONTENT

Supporting Information

Additional FTIR spectra of O_2-treated CaI and O_2-treatment of H_{ox}, H_{red}-DT, and CO-inhibited CrHydA1, CrHydA1 activity, and HydF titration data, peptide map and MS data for Cys169, experimental conditions summary table, and crystallographic data collection and refinement statistics for O_2-exposed CrHydA1. This material is available free of charge via the Internet at http://pubs.acs.org.

AUTHOR INFORMATION

Corresponding Authors

*paul.king@nrel.gov
*john.peters@chemistry.montana.edu

Author Contributions

§These authors contributed equally.

Notes

The authors declare no competing financial interest.

ACKNOWLEDGMENTS

J.W.P. thanks the Air Force Office of Scientific Research grant 574 FA-9550-11-1-0218 for supporting work on the mechanism of oxygen sensitivity. M.W.R., D.W.M., and P.W.K. gratefully acknowledge funding support for CrHydA1 and CaI preparation and FTIR spectra measurements from the U.S. Department of Energy, Office of Science, Basic Energy Sciences, Division of Chemical Sciences, Geosciences, and Biosciences and support of the U.S. Department of Energy under contract no. DE-AC36-08-GO28308 with the National Renewable Energy Laboratory. The work on reactivation of damaged CrHydA1 with purified HydF was supported by the U.S. Department of Energy grant DE-FG02-10ER16194 (to J.B.B. and J.W.P.). Use of the Stanford Synchrotron Radiation Lightsource, SLAC National Accelerator Laboratory, is supported by the U.S. Department of Energy, Office of Science, Office of Basic Energy Sciences under contract no. DE-AC02-76SF00515. The SSRL Structural Molecular Biology Program is supported by the DOE Office of Biological and Environmental Research, and by the National Institutes of Health, National Institute of General Medical Sciences (including P41GM103393). The mass spectrometry facility at MSU receives funding from the Murdock Charitable Trust and NIH 5P20RR02437 of the Cobre program. The contents of this publication are solely the responsibility of the authors and do not necessarily represent the official views of NIGMS or NIH. Atomic coordinates were deposited in the PDB (code, 4ROV).

REFERENCES

(1) Vignais, P. M.; Billoud, B. *Chem. Rev.* **2007**, *107* (10), 4206−4272.
(2) McKinlay, J. B.; Harwood, C. S. *Curr. Opin. Biotechnol.* **2010**, *21* (3), 244−251.
(3) Turner, J.; Sverdrup, G.; Mann, M. K.; Maness, P.-C.; Kroposki, B.; Ghirardi, M.; Evans, R. J.; Blake, D. *Int. J. Energy Res.* **2008**, *32* (5), 379−407.
(4) Nicolet, Y.; Piras, C.; Legrand, P.; Hatchikian, C. E.; Fontecilla-Camps, J. C. *Structure* **1999**, *7* (1), 13−23.
(5) Peters, J. W.; Lanzilotta, W. N.; Lemon, B. J.; Seefeldt, L. C. *Science* **1998**, *282* (5395), 1853−1858.
(6) Pandey, A. S.; Harris, T. V.; Giles, L. J.; Peters, J. W.; Szilagyi, R. K. *J. Am. Chem. Soc.* **2008**, *130* (13), 4533−4540.
(7) Silakov, A.; Wenk, B.; Reijerse, E.; Lubitz, W. *Phys. Chem. Chem. Phys.* **2009**, *11* (31), 6592−6599.
(8) Berggren, G.; Adamska, A.; Lambertz, C.; Simmons, T. R.; Esselborn, J.; Atta, M.; Gambarelli, S.; Mouesca, J. M.; Reijerse, E.; Lubitz, W.; Happe, T.; Artero, V.; Fontecave, M. *Nature* **2013**, *499* (7456), 66−69.
(9) Ghirardi, M. L.; Posewitz, M. C.; Maness, P.-C.; Dubini, A.; Yu, J.; Seibert, M. *Annu. Rev. Plant Biol.* **2007**, *58* (1), 71−91.
(10) Melis, A.; Seibert, M.; Happe, T. *Photosynth. Res.* **2004**, *82* (3), 277−288.
(11) Erbes, D. L.; King, D.; Gibbs, M. *Plant Physiol.* **1979**, *63* (6), 1138−1142.
(12) Cohen, J.; Kim, K.; Posewitz, M.; Ghirardi, M. L.; Schulten, K.; Seibert, M.; King, P. *Biochem. Soc. Trans.* **2005**, *33* (Pt1), 80−82.
(13) Liebgott, P.-P.; Leroux, F.; Burlat, B.; Dementin, S.; Baffert, C.; Lautier, T.; Fourmond, V.; Ceccaldi, P.; Cavazza, C.; Meynial-Salles, I.; Soucaille, P.; Fontecilla-Camps, J. C.; Guigliarelli, B.; Bertrand, P.; Rousset, M.; Léger, C. *Nat. Chem. Biol.* **2010**, *6* (1), 63−70.
(14) Baffert, C.; Demuez, M.; Cournac, L.; Burlat, B.; Guigliarelli, B.; Bertrand, P.; Girbal, L.; Léger, C. *Angew. Chem., Int. Ed.* **2008**, *47* (11), 2052−2054.
(15) Goldet, G.; Brandmayr, C.; Stripp, S. T.; Happe, T.; Cavazza, C.; Fontecilla-Camps, J. C.; Armstrong, F. A. *J. Am. Chem. Soc.* **2009**, *131* (41), 14979−14989.

DOI: 10.1021/ja510169s
J. Am. Chem. Soc. 2015, 137, 1809−1816

(16) Vincent, K. A.; Parkin, A.; Lenz, O.; Albracht, S. P. J.; Fontecilla-Camps, J. C.; Cammack, R.; Friedrich, B.; Armstrong, F. A. *J. Am. Chem. Soc.* **2005**, *127* (51), 18179−18189.
(17) Cohen, J.; Kim, K.; King, P. W.; Seibert, M.; Schulten, K. *Structure* **2005**, *13* (9), 1321−1329.
(18) Lautier, T.; Ezanno, P.; Baffert, C.; Fourmond, V.; Cournac, L.; Fontecilla-Camps, J. C.; Soucaille, P.; Bertrand, P.; Meynial-Salles, I.; Leger, C. *Faraday Discuss.* **2011**, *148* (0), 385−407.
(19) Nicolet, Y.; Cavazza, C.; Fontecilla-Camps, J. C. *J. Inorg. Biochem.* **2002**, *91* (1), 1−8.
(20) Bruska, M. K.; Stiebritz, M. T.; Reiher, M. *J. Am. Chem. Soc.* **2011**, *133* (50), 20588−20603.
(21) Stiebritz, M. T.; Reiher, M. *Chem. Sci.* **2012**, *3* (6), 1739−1751.
(22) Kubas, A.; De Sancho, D.; Best, R. B.; Blumberger, J. *Angew. Chem., Int. Ed.* **2014**, *126* (16), 4165−4168.
(23) Finkelmann, A. R.; Stiebritz, M. T.; Reiher, M. *Inorg. Chem.* **2014**, *53* (22), 11890−11902.
(24) Hong, G.; Pachter, R. *ACS Chem. Biol.* **2012**, *7* (7), 1268−1275.
(25) Dey, S.; Rana, A.; Crouthers, D.; Mondal, B.; Das, P. K.; Darensbourg, M. Y.; Dey, A. *J. Am. Chem. Soc.* **2014**, *136* (25), 8847−8850.
(26) Fourmond, V.; Greco, C.; Sybirna, K.; Baffert, C.; Wang, P.-H.; Ezanno, P.; Montefiori, M.; Bruschi, M.; Meynial-Salles, I.; Soucaille, P.; Blumberger, J.; Bottin, H.; De Gioia, L.; Léger, C. *Nat. Chem.* **2014**, *6* (4), 336−342.
(27) Stripp, S. T.; Goldet, G.; Brandmayr, C.; Sanganas, O.; Vincent, K. A.; Haumann, M.; Armstrong, F. A.; Happe, T. *Proc. Natl. Acad. Sci. U.S.A.* **2009**, *106* (41), 17331−17336.
(28) Lambertz, C.; Leidel, N.; Havelius, K. G. V.; Noth, J.; Chernev, P.; Winkler, M.; Happe, T.; Haumann, M. *J. Biol. Chem.* **2011**, *286*, 40614−40623.
(29) Greco, C.; Fourmond, V.; Baffert, C.; Wang, P.-h.; Dementin, S.; Bertrand, P.; Bruschi, M.; Blumberger, J.; de Gioia, L.; Leger, C. *Energy Environ. Sci.* **2014**, *7* (11), 3543−3573.
(30) King, P. W.; Posewitz, M. C.; Ghirardi, M. L.; Seibert, M. *J. Bacteriol.* **2006**, *188* (6), 2163−2172.
(31) Yacoby, I.; Tegler, L. T.; Pochekailov, S.; Zhang, S.; King, P. W. *PLoS One* **2012**, *7* (4), e35886.
(32) McGlynn, S. E.; Shepard, E. M.; Winslow, M. A.; Naumov, A. V.; Duschene, K. S.; Posewitz, M. C.; Broderick, W. E.; Broderick, J. B.; Peters, J. W. *FEBS Lett.* **2008**, *582* (15), 2183−2187.
(33) Mulder, D. W.; Ratzloff, M. W.; Shepard, E. M.; Byer, A. S.; Noone, S. M.; Peters, J. W.; Broderick, J. B.; King, P. W. *J. Am. Chem. Soc.* **2013**, *135* (18), 6921−6929.
(34) Kabsch, W. *Acta Crystallogr., Sect. D: Biol. Crystallogr.* **2010**, *66* (2), 125−132.
(35) Evans, P. *Acta Crystallogr., Sect. D: Biol. Crystallogr.* **2006**, *62* (1), 72−82.
(36) Vagin, A.; Teplyakov, A. *J. Appl. Crystallogr.* **1997**, *30* (6), 1022−1025.
(37) Pierik, A. J.; Hulstein, M.; Hagen, W. R.; Albracht, S. P. J. *Eur. J. Biochem.* **1998**, *258* (2), 572−578.
(38) Roseboom, W.; De Lacey, A.; Fernandez, V.; Hatchikian, E. C.; Albracht, S. J. *J. Biol. Inorg. Chem.* **2006**, *11* (1), 102−118.
(39) Chen, Z. J.; Lemon, B. J.; Huang, S.; Swartz, D. J.; Peters, J. W.; Bagley, K. A. *Biochemistry* **2002**, *41* (6), 2036−2043.
(40) Bennett, B.; Lemon, B. J.; Peters, J. W. *Biochemistry* **2000**, *39* (25), 7455−7460.
(41) Adamska, A.; Silakov, A.; Lambertz, C.; Rüdiger, O.; Happe, T.; Reijerse, E.; Lubitz, W. *Angew. Chem., Int. Ed.* **2012**, *51* (46), 11458−11462.
(42) Silakov, A.; Kamp, C.; Reijerse, E.; Happe, T.; Lubitz, W. *Biochemistry* **2009**, *48* (33), 7780−7786.
(43) Liu, T.; Li, B.; Singleton, M. L.; Hall, M. B.; Darensbourg, M. Y. *J. Am. Chem. Soc.* **2009**, *131* (23), 8296−8307.
(44) Stiebritz, M. T.; Reiher, M. *Inorg. Chem.* **2009**, *48* (15), 7127−7140.
(45) Stiebritz, M. T.; Finkelmann, A. R.; Reiher, M. *Eur. J. Inorg. Chem.* **2011**, *2011* (7), 1163−1171.
(46) Mulder, D. W.; Ortillo, D. O.; Gardenghi, D. J.; Naumov, A. V.; Ruebush, S. S.; Szilagyi, R. K.; Huynh, B.; Broderick, J. B.; Peters, J. W. *Biochemistry* **2009**, *48* (26), 6240−6248.
(47) Mulder, D. W.; Boyd, E. S.; Sarma, R.; Lange, R. K.; Endrizzi, J. A.; Broderick, J. B.; Peters, J. W. *Nature* **2010**, *465* (7295), 248−251.
(48) Nicolet, Y.; Rohac, R.; Martin, L.; Fontecilla-Camps, J. C. *Proc. Natl. Acad. Sci. U.S.A.* **2013**, *110* (18), 7188−7192.
(49) Cornish, A. J.; Gärtner, K.; Yang, H.; Peters, J. W.; Hegg, E. L. *J. Biol. Inorg. Chem.* **2011**, *286* (44), 38341−38347.
(50) Mulder, D. W.; Ratzloff, M. W.; Bruschi, M.; Greco, C.; Koonce, E.; Peters, J. W.; King, P. W. *J. Am. Chem. Soc.* **2014**, *136* (43), 15394−15402.

DOI: 10.1021/ja510169s
J. Am. Chem. Soc. 2015, 137, 1809−1816